2009 IEEE International Conference on Robotics and Automation
Kobe International Conference Center
Kobe, Japan, May 12-17, 2009

Decoupled visual servoing based on the spherical projection of a set of points

Hicham Hadj-Abdelkader, Youcef Mezouar and Philippe Martinet

***Abstract*— This paper extends the recent work proposed in [21]. In this work, it has been noted that three visual features (to control three degrees of freedom) obtained from the spherical projection of 3D spheres allows nice decoupling properties and global stability. However, even if such an approach is theoretically attractive, it is limited by a major practical issue since spherical objects have to be observed while only three degrees of freedom can be controlled. In this paper, we show that similar properties can be obtained by observing a set of points. The basic idea is to build a virtual 3D sphere from two 3D points and to analyse its related spherical projection. Furthermore, to control the six degrees of freedom a 2D 1/2 control scheme is proposed which allows us to fully decouple rotational motions from translational motions.**

I. INTRODUCTION

In vision-based control, the choice of the set of visual features to be used in the control scheme is still an open question, despite of the large quantity of results obtained in the last few years. Several kinds of visual servoing can be distinguished, according to the space where the visual features were defined. In position-based visual servo (PBVS) [22], the features are defined in the 3D space. The control scheme using PBVS ensures a nice decoupling between the degrees of freedom (dofs)(refer to [1]). For this reason, adequate 3D trajectories can be obtained, such as a geodesic for the orientation and a straight line for the translation. However, position-based visual servoing may suffer from potential instabilities due to image noise [3]. On the opposite, in image-based visual servo (IBVS) [7], the visual servo is performed in the image. Whatever the nature of the possible measures extracted from the image, whether it be a set of image points coordinates or a set of image moments, the main question is how to combine them to obtain an adequate behavior of the system. In most works, the combination of different features is nothing but a simple stacking. If the error between the initial value of the features and the desired one is small, and if the task to realize constrains all the available degrees of freedom (dofs), that may be a good choice. However, as soon as the error is large, problems may appear such as reaching local minimum or task singularities [3].

The way to design adequate visual features is directly linked to the modeling of their interaction with the robot motion, from which all control properties can be analyzed theoretically. If the interaction is too complex (i.e. highly non linear and coupled), the analysis becomes impossible and the behavior of the system is generally not satisfactory in difficult configurations where large displacements (especially rotational ones) have to be realized. To overcome these problems, it is possible to combine path planning and visual servoing, since tracking planned trajectories allows the error to always remain small [17]. A second approach is to use the measures to build particular visual features that will ensure expected properties of the control scheme. Several works have been realized in image-based visual servoing following the same general objective. In [18], a vanishing point and the horizon line have been selected. This choice ensures a good decoupling between translational and rotational dofs. In [13], vanishing points have also been used for a dedicated object (a 3D rectangle), once again for decoupling properties. For the same object, six visual features have been designed in [5] to control the six dofs of a robot arm, following a partitioned approach. In [12], the coordinates of points are expressed in a cylindrical coordinate system instead of the classical Cartesian one, so as to improve the robot trajectory. In [11], the three coordinates of the centroid of an object in a virtual image obtained through a spherical projection have been selected to control three dofs of an under-actuated system. By selecting an adequate combination of moments, it is also possible to determine partitioned systems with good decoupling and linearizing properties when considering planar objects [4] or non planar objects [20].

Recently, in [21] three visual features which allows nice decoupling properties and global stability even in the presence of modeling errors, have been proposed. The proposed approach is based on image features obtained from the projection onto a unit sphere of 3D spheres. As a consequence of the use of a spherical projection, the obtained results are valid for any sensor obeying the unified camera model. In other words, it encompasses all sensors in this class [9]: perspective and catadioptric. Some class of fisheye cameras can also be concerned by this model [6]. However, even if such an approach is theoretically attractive, it is limited by a major practical issue since spherical objects have to be observed while only three degrees of freedom can be controlled. In this paper, we show that similar decoupling properties can be obtained by observing a set of points. The basic idea is to build a virtual 3D sphere from two 3D points and to analyse its related spherical projection. We also show that the system remains globally stable even in the presence of modeling errors. Furthermore, to control the six degrees of freedom a 2D 1/2 control scheme is presented allowing a new decoupled control scheme from the spherical projection of a set of points.

Authors are with LASMEA UMR 6602 CNRS, 24 avenue des Landais - 63177 Aubiere Cedex - France {hadj,mezouar,martinet}@univ-bpclermont.fr

II. MODELISATION

In this section, we recall the unified central projection using the unitary sphere. Then, we present the geometric relation between visual features related to 3D points and spheres.

A. Unified central projection

Central imaging systems can be modeled using two consecutive projections: spherical projection and perspective one. This geometric formulation called unified model has been proposed by Geyer and Daniilidis in [8] and has been intensively used by the vision and robotics community (structure from motion, calibration, visual servoing, ...).

We recall, in this section, the unified central projection model. Consider the virtual unitary sphere centered in M as shown in Fig.1 and the perspective camera centered in C. The frames attached to the spherical mirror and the perspective camera are related by a simple translation of $-\xi$ along the Z axis. Let $\mathcal{X}$ be a 3D point with coordinates $\mathbf{X} = [X\ Y\ Z]^\top$ in $\mathcal{F}_m$. The world point $\mathcal{X}$ is projected in the image plane into the point of homogeneous coordinates $\mathbf{x_i} = [x_i\ y_i\ 1]^\top$. The image formation process can be split in three steps given in the following:

- First step: The 3D world point $\mathcal{X}$ is first mapped onto the unit sphere surface:

$$\mathbf{X_m} = \frac{1}{\rho}\left[\begin{array}{ccc} \mathrm{X} & \mathrm{Y} & \mathrm{Z} \end{array}\right]^\top$$

where $\rho = \|\mathbf{X}\| = \sqrt{X^2+Y^2+Z^2}$.

- Second step: The point $\mathbf{X_m}$ lying on the unitary sphere is then perspectively projected on the normalized image plane $Z = 1-\xi$ in to a point of homogeneous coordinates:

$$\underline{\mathbf{x}} = \mathbf{f}(\mathbf{X}) = \left[\begin{array}{ccc} \dfrac{X}{Z+\xi\rho} & \dfrac{Y}{Z+\xi\rho} & 1 \end{array}\right]^\top \quad (1)$$

- Last step: The 2D projective point $\underline{\mathbf{x}}$ is mapped into the pixel image point with homogeneous coordinates $\underline{\mathbf{x_i}}$ using the collineation matrix $\mathbf{K}$:

$$\underline{\mathbf{x_i}} = \mathbf{K}\underline{\mathbf{x}}$$

The matrix $\mathbf{K}$ contains the conventional camera intrinsic parameters coupled with mirror intrinsic parameters. It can be written as:

$$\mathbf{K} = \begin{bmatrix} f_u & \alpha_{uv} & u_0 \\ 0 & f_v & v_0 \\ 0 & 0 & 1 \end{bmatrix}$$

The matrix $\mathbf{K}$ and the parameter ξ can be obtained after calibration using for examples the methods proposed in [2]. In the sequel, the central imaging system is considered calibrated. In this case, the inverse projection onto the unit sphere can be obtained by inverting the second and last steps. As a matter of fact, the point $\underline{\mathbf{x}}$ in the normalized image plane is obtained using the inverse mapping $\mathbf{K^{-1}}$:

$$\underline{\mathbf{x}} = [x\ y\ 1]^\top = \mathbf{K^{-1}}\underline{\mathbf{x_i}} \quad (2)$$

The point onto the unit sphere is then obtained by inverting the non-linear projection equation (1):

$$\mathbf{X_m} = \mathbf{f^{-1}}(\underline{\mathbf{x}}) = \lambda\left[x\ y\ 1-\frac{\xi}{\lambda}\right]^\top \quad (3)$$

where $\lambda = \dfrac{\xi+\sqrt{1+(1-\xi^2)(x^2+y^2)}}{x^2+y^2+1}$.

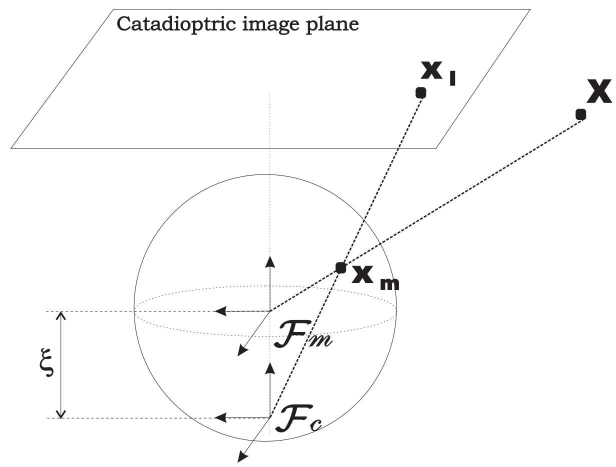

Fig. 1. Unified central projection

As can be shown in equation (1), the perspective projection model is obtained by setting $\xi = 0$.

B. Virtual sphere projection through two 3D points

In this section we present the central projection of a virtual sphere through two points in the 3D space. This formulation should be interesting to extract potential visual features as presented in [21].

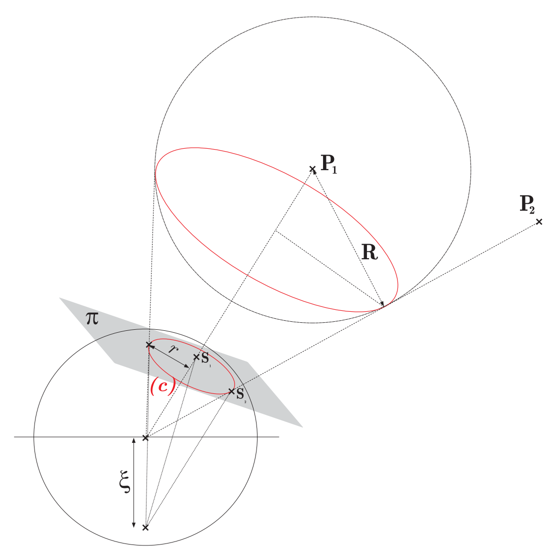

Fig. 2. Projection model of a virtual sphere

Let $\mathcal{P}_1$ and $\mathcal{P}_2$ be two 3D points with coordinates $\mathbf{P_1} = [X_1\ Y_1\ Z_1]^\top$ and $\mathbf{P_2} = [X_2\ Y_2\ Z_2]^\top$ with respect to the unitary mirror frame $\mathcal{F}_m$. These points are viewed in two points $\mathbf{p_1}$ and $\mathbf{p_2}$ in the image plane. Using equations (2) and (3), the coordinates of the points $\mathbf{S_1}$ and $\mathbf{S_2}$ onto the unit sphere can be obtained from image points coordinates $\mathbf{p_1}$ and $\mathbf{p_2}$ respectively.

Consider now a virtual sphere $\mathcal{S}(\mathcal{P}_1, R)$ of center the 3D point $\mathcal{P}_1$ and radius R ($R \in \mathcal{R}^+$). The sphere $\mathcal{S}$ is virtual and its radius R is constrained by the distance between the sphere center $\mathcal{P}_1$ and the ray projection of the point $\mathcal{P}_2$ passing through the center M of the unitary sphere (see figure 2).

By assuming the first step of the central projection model, the occluding contour of the virtual sphere $\mathcal{S}(\mathcal{P}_1, R)$ is projected to a small circle (c) onto the unitary spherical mirror. This small circle (c) lies on a plane (π), called interpretation plane, defined by its unit normal vector $\underline{\mathbf{n}} = [n_x\ n_y\ n_z]^\top$ and its distance d from the center M. So, any point in (c) with coordinates $[X\ Y\ Z]^\top$ expressed in the mirror frame $\mathcal{F}_m$ satisfies the unit sphere and plane equations:

$$(c) : \begin{cases} X^2 + Y^2 + Z^2 = 1 \\ n_x X + n_y Y + n_z Z - d = 0 \end{cases} \tag{4}$$

Note that a line in 3D space is projected to a great circle since the interpretation plane passes through the center M where $d = 0$ (refer to [2]). Therefore, the equations for central projection of spheres and lines can be represented in a unified framework.

From figure 2, it is easy to show that the vector coordinates $\mathbf{S_1}$ (the spherical projection of $\mathcal{P}_1$ onto the unit sphere) is normal to the plane (π). The normal vector $\underline{\mathbf{n}}$ can thus be computed through the inverse projection onto the unit sphere.

In [21], the radius r of the small circle (c) is written as:

$$r = \frac{R}{\|\mathbf{P_1}\|} = \frac{R}{\sqrt{X_1^2 + Y_1^2 + Z_1^2}} \tag{5}$$

Since the sphere $\mathcal{S}(\mathcal{P}_1, R)$ is constrained by the points $\mathcal{P}_1$ and $\mathcal{P}_2$, the radius r can easily be obtained from the angular distance between $\mathcal{P}_1$ and $\mathcal{P}_2$ and thus between $\mathbf{S_1}$ and $\mathbf{S_2}$:

$$\begin{aligned} r &= \sin(\cos^{-1}(\mathbf{S_1}^\top \mathbf{S_2})) \\ &= \sqrt{1 - (\mathbf{S_1}^\top \mathbf{S_2})^2} \end{aligned} \tag{6}$$

Hence, from two points observed by a central camera, circle parameters related to the projection of a virtual sphere can be obtained. These parameters can be calculated in the image plane or on the unit sphere since the camera calibration is supposed known.

III. VISUAL SERVOING

In this section, we present a hybrid visual servoing scheme to control the 6 dofs of the camera. As usual when designing a 2 1/2 D visual servoing, the feature vector used as input of the control law combines 2-D and 3-D informations [15], [10]:

$$\mathbf{s} = [\mathbf{s_1}^\top\ \ \theta\mathbf{u}^\top]^\top$$

where $\mathbf{s}_1$ is a 3-dimensional vector containing the 2D features and, $\mathbf{u}$ and θ are respectively the axis and the rotation angle obtained between the current and desired camera situations. The rotation parameters can be obtained from an homography matrix $\mathbf{H}$ related to a reference plane observed by a central camera [10]. The matrix $\mathbf{H}$ can usually be estimated up to a scale factor using at least four coplanar observed points. Otherwise, three points are chosen to define the reference plane and at least five supplementary points are necessary to estimate the homography matrix by using for example the linear algorithm proposed in [14].

Recently, Tatsambon and Chaumette show in [21] that similar decoupling properties to those obtained with 3D points [16] can be obtained by combining visual features related to the spherical projection of a sphere. Let us now choose $\mathbf{s_1} = \frac{1}{r}\mathbf{S_1} = \frac{1}{r}[X_{s1}\ Y_{s1}\ Z_{s1}]^\top$ as the 3-dimensional vector containing the 2D features. These parameters can be estimated from a set of two points (defining a virtual sphere) as explained in the previous Section. The task function $\mathbf{e}$ to regulate to 0 [19] is given by: $\mathbf{e} = \mathbf{s} - \mathbf{s}^*$ where $\mathbf{s}^*$ is the desired value of $\mathbf{s}$. The exponential decay of $\mathbf{e}$ toward $\mathbf{0}$ can be obtained by imposing $\dot{\mathbf{e}} = -\lambda\mathbf{e}$ (λ being a proportional gain), the corresponding control law is:

$$\tau = -\lambda\mathbf{L}^{-1}(\mathbf{s} - \mathbf{s}^*) \tag{7}$$

where τ is a 6-dimensional vector denoting the velocity screw of the camera. It contains the instantaneous angular velocity ω and the instantaneous linear velocity v. $\mathbf{L}$ is the interaction matrix related to $\mathbf{s}$. It links the variation of $\mathbf{s}$ to the camera velocity: $\dot{\mathbf{s}} = \mathbf{L}\tau$. It is thus necessary to compute the interaction matrix in order to derive the control law given by the Equation (7). At this aim, we can follow a similar reasoning that in [21].First, the time derivative of the vector $\mathbf{s_1}$ can be decomposed as:

$$\dot{\mathbf{s}}_\mathbf{1} = \frac{r\dot{\mathbf{S}}_\mathbf{1} - \mathbf{S_1}\,\dot{r}}{r^2} \tag{8}$$

The time derivative of the radius r can be obtained from the equation (5):

$$\dot{r} = \mathbf{L}_r\tau = \begin{pmatrix} \frac{r^2}{R}\mathbf{S_1}^\top & \mathbf{0_{1\times3}} \end{pmatrix}\tau \tag{9}$$

After few developments, we get the time derivative of the spherical point $\mathbf{S_1}$:

$$\dot{\mathbf{S}}_\mathbf{1} = \mathbf{L}_{\mathbf{S_1}}\tau = \begin{pmatrix} \frac{r}{R}(\mathbf{S_1}\mathbf{S_1}^\top - \mathbf{I_3}) & [\mathbf{S_1}]_\times \end{pmatrix}\tau \tag{10}$$

where $[\mathbf{S_1}]_\times$ is the antisymmetric matrix related to the vector $\mathbf{S_1}$. According to equations (9) and (10), equation (8) can be rewritten as:

$$\dot{\mathbf{s}}_\mathbf{1} = \mathbf{L}_{\mathbf{s_1}}\tau$$

where

$$\mathbf{L}_{\mathbf{s_1}} = \begin{pmatrix} \mathbf{L_{s1}}_{v} & \mathbf{L_{s1}}_{\omega} \end{pmatrix} \tag{11}$$

and

$$\mathbf{L_{s1}}_{\upsilon} = \begin{pmatrix} -\frac{1}{R} & 0 & 0 \\ 0 & -\frac{1}{R} & 0 \\ 0 & 0 & -\frac{1}{R} \end{pmatrix}$$
$$\mathbf{L_{s1}}_{\omega} = \begin{pmatrix} 0 & -\frac{Z_{s1}}{r} & \frac{Y_{s1}}{r} \\ \frac{Z_{s1}}{r} & 0 & -\frac{X_{s1}}{r} \\ -\frac{Y_{s1}}{r} & \frac{X_{s1}}{r} & 0 \end{pmatrix} \tag{12}$$

As can be shown in $\mathbf{L_{s1}}$, the only unknown parameter is the radius R of the virtual sphere which appears as a gain on the translational velocities. When a real sphere is observed, an estimated value $\widehat{R}$ of the real radius R can be used. However, in the considered case the radius R varies when moving the camera and/or the two points selected to define the virtual sphere (except for some configuration as for example when the point $\mathcal{P}_2$ moves along the projection ray). Fortunately, a non-zero positive value attributed to R should insure the global stability of the control law [21]. Indeed, if we choose $\widehat{R}$ as a positive constant value, the global asymptotic stability is guaranteed and the scale factor between the real radius R and the estimated one $\widehat{R}$ appears as an over-gain in the translational velocities.

Concerning the rotation vector $\theta\mathbf{u}$, its time derivative can be expressed as a function of the camera velocity screw:

$$\frac{d(\theta\mathbf{u})}{dt} = \begin{pmatrix} \mathbf{0_3} & \mathbf{L}_{\omega} \end{pmatrix} \tau \tag{13}$$

where $\mathbf{L}_{\omega}$ is given in [15]:

$$\mathbf{L}_{\omega} = \mathbf{I_3} - \frac{\theta}{2}[\mathbf{u}]_{\times} + \left(1 - \frac{\mathrm{sinc}(\theta)}{\mathrm{sinc}^2(\frac{\theta}{2})}\right)[\mathbf{u}]^2_{\times} \tag{14}$$

and $\mathrm{sinc}(\theta) = \dfrac{\sin(\theta)}{\theta}$.

Finally, according to equations (11) and (13), the global interaction matrix related to $\mathbf{s} = [\mathbf{s_1}^\top \ \ \theta\mathbf{u}^\top]^\top$ is given by:

$$\mathbf{L_s} = \begin{pmatrix} \mathbf{L_{s1}}_{\upsilon} & \mathbf{L_{s1}}_{\omega} \\ \mathbf{0_3} & \mathbf{L}_{\omega} \end{pmatrix} \tag{15}$$

In practice, an approximated interaction matrix $\widehat{\mathbf{L}}$ is used to compute the control vector (7):

$$\tau = -\lambda \begin{pmatrix} \widehat{\mathbf{L}}^{-1}_{\mathbf{s1}\upsilon} & -\widehat{\mathbf{L}}^{-1}_{\mathbf{s1}\upsilon}\mathbf{L_{s1}}_{\omega}\widehat{\mathbf{L}}^{-1}_{\omega} \\ \mathbf{0_3} & \widehat{\mathbf{L}}^{-1}_{\omega} \end{pmatrix} (\mathbf{s} - \mathbf{s}^*) \tag{16}$$

Note also that one can set $\widehat{\mathbf{L}}^{-1}_{\omega}$ to $\mathbf{I_3}$ since [15]:

$$\widehat{\mathbf{L}}^{-1}_{\omega}\ \widehat{\theta\mathbf{u}} = \widehat{\theta\mathbf{u}}$$

IV. RESULTS

We present now results concerning a positioning task of the six degrees of freedom of a camera using the previously described control scheme. In the two first experiments, two different types of central cameras are used, *i.e* a conventional camera and a catadioptric camera (combination of mirror and conventional camera). The motion in these experiments is generic (translation and rotation motion). In the third experiment, we show the benefit of decoupling rotational motions from translational motions. We show in the last one the gain effect on the translation velocities occurred by the distance between the two points chosen for creating the virtual sphere. For all experiments, the observed target is composed by a set of coplanar points, the control gain is set to $\lambda = 0.1$ and the radius $\widehat{R}$ is set to 0.2.

To be close to a real setup, uniform distribution random noise of variance $2 pixels$ has been added to the correct pixel coordinates, and the calibration errors are simulated by adding an error of 10% to the real camera parameters.

A. Experiment 1

In this experiment, a conventional camera with calibration parameters $f_u = f_v = 900$, $f_{uv} = 0$, $u_0 = 652$ and $v_0 = 511$ is used. For this type of camera, the parameter ξ is equal to 0. The displacement between the initial and desired camera frames is given by the translation $\mathbf{t} = [1 \ \ 0.7 \ \ 0.7]^\top$ m and the rotation $\theta\mathbf{u} = [0 \ \ 0 \ \ 178]^\top$ degree.

As can been noticed on Figure 3, the positioning task is correctly realized despite image noises, erroneous calibration parameters and unknown variable radius of the virtual sphere. The correct regulation to zero of the components of $\mathbf{s} - \mathbf{s}^*$ can be observed in 3(b). The current points in the image reach their desired positions in the image plane. The corresponding trajectories in the image are shown in Figure 3(a). As can be seen in Figures 3(c) and 3(d) which correspond to the translational and rotational camera velocities, the rotational motions are, as expected, perfectly decoupled from the translational motions.

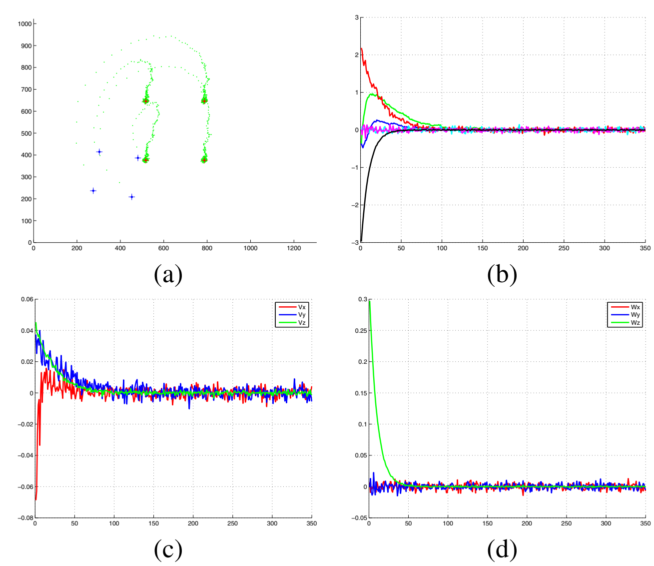

Fig. 3. Experiment 1 with a perspective camera: (a) trajectory of points on the image, (b) errors vector, (c) translational velocities given in m/s, (d) rotational velocities given in rad/s

B. Experiment 2

Now, we present simulation results when using a catadioptric camera. The calibration parameters are given by $f_u = f_v = 303$, $f_{uv} = 0$, $u_0 = 652$, $v_0 = 511$ and $\xi = 1$. The displacement between the initial and desired camera positions is given by the translation $\mathbf{t} = [0 \;\; 1 \;\; 0]^\top$ m and the rotation $\theta\mathbf{u} = [0 \;\; 60 \;\; 120]^\top$ degree.

Noise and modelling errors are set as in the previous experiments. Once again, the positioning task is properly realized. The errors vector, plotted in Figure 4(b), converges to zero and thus the current image coincides with the desired one at convergence (see Figure 4(a)). The Figures 4(c) and 4(d) representing the translational and rotational velocities show that the rotational errors are corrected before the translational ones. Indeed, the actual radius R of the virtual sphere varies during the motion while $\widehat{R}$ is set as a constant value to evaluate the interaction matrix $\mathbf{L_s}$.

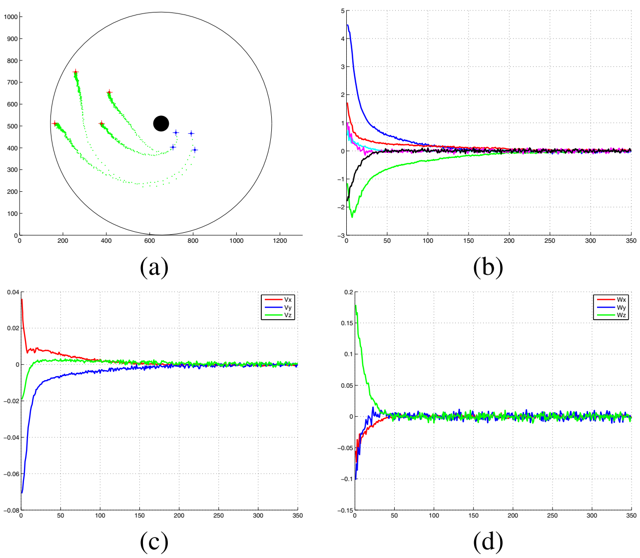

Fig. 4. Experiment 2 with a catadioptric camera: (a) trajectory of points on the image, (b) errors vector, (c) translational velocities given in m/s, (d) rotational velocities given in rad/s

C. Experiment 3

In this experiment, we show the benefit of decoupling rotational motions from the translational motions. Indeed, for a positioning task corresponding to a pure translation, rotational velocities in the control law (16) are not affected. However, modelling errors and image noises can affect the decoupling properties. To illustrate this point, we consider a pure translational motion of $\mathbf{t_1} = [2 \;\; 1 \;\; -2]^\top$ m for the perspective camera and of $\mathbf{t_2} = [-0.5 \;\; 2.6 \;\; -0.5]^\top$ m for the catadioptric camera. Results of this experiment are plotted on Figures 5 where left figures and right figures correspond to the perspective and catadioptric cameras respectively. Image trajectories are shown in Figures 5(a) and 5(b). The translational and rotational velocities shown in Figures 5(c,d) and 5(e,f) confirm the decoupling and the robustness of the proposed approach.

D. Experiment 4

Recall that 2 image points are necessary to generate a virtual sphere. In this last experiment, we show how the choice of these points affect the translational velocities. The displacements between the initial and desired camera frames

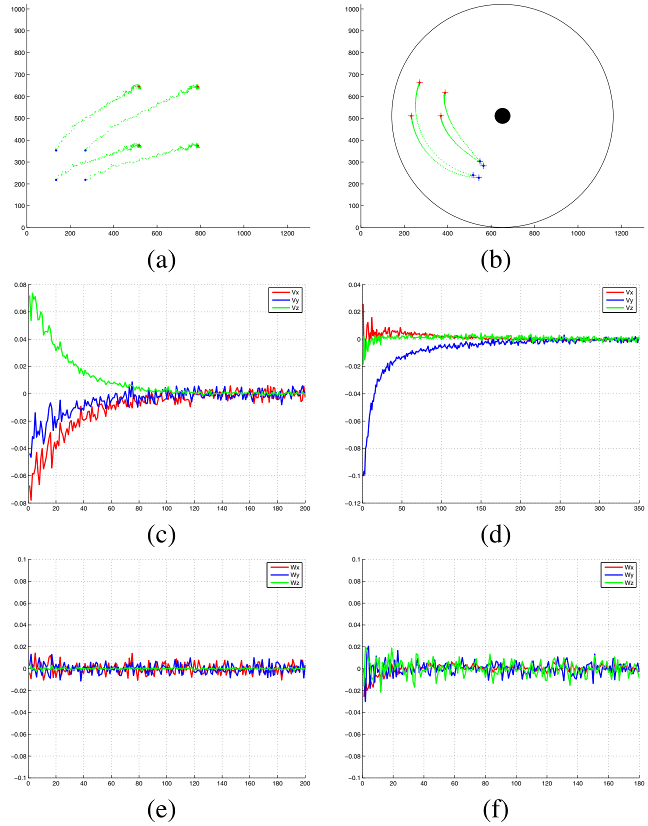

Fig. 5. Experiment 3: pure translation: (a) and (b) image trajectories, (c) and (d)) translational velocities given in m/s, (e) and (f) rotational velocities given in rad/s

are chosen as those used in experiments 1 and 2 for the perspective and catadioptric cameras respectively. Since the translation velocities are linked to the observation vector $\mathbf{s_1}$ by the radius R, the distance between two points in the image, selected to define the virtual sphere, has an over-gain effect on the translation control. Two pairings are considered in this experiments. The first pairing is chosen as the two closest points while the second pairing is chosen as the farthest points in the image. Figure 6 (respectively Figure 7) shows the translational and rotational velocities of the perspective camera (respectively catadioptric camera). Results corresponding to the closest points are presented on the left column and results related to the farthest points in the right column. As can be observed in the translational velocities, the gain on the translational velocities substantially increase when the closest points are chosen to define the virtual sphere. Indeed, the distance between the two points in the image is proportional to the radius of the virtual sphere and thus inversely proportional to the translational control gain. Rotational velocities curves shown in Figures 6 and 7 are not changed since the radius R appear only in the translation control and the first point selected as the virtual sphere center is chosen the same for the both pairings.

V. CONCLUSIONS AND FUTURE WORKS

In this paper we have mainly extended the recent work proposed in [21]. Indeed the proposed approach ensuring nice decoupling properties and global stability, was limited by major practical issues since spherical objects have to be observed while only three degrees of freedom can be controlled. We have shown that similar properties can be obtained by observing a set of points which significantly increases the potential application of such a control scheme. Furthermore, the 2D features obtained from two points have been used in a 2D 1/2 control scheme to fully control and decouple the 3 rotational dofs from the 3 translational ones. We are currently working on obtaining a similar behavior using a pure 2D control scheme.

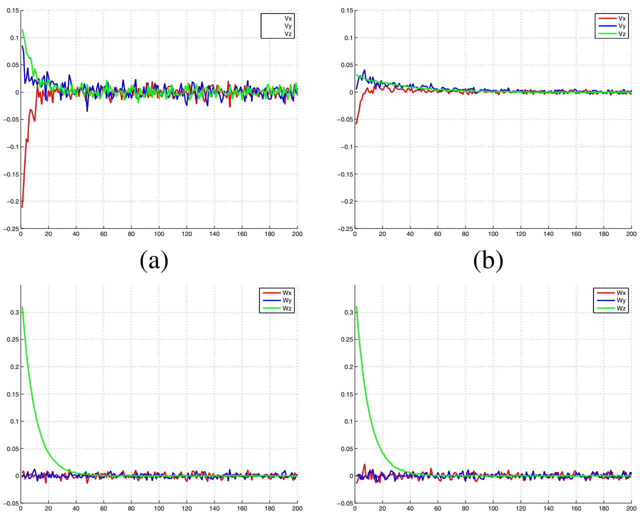

(a) (b) (c) (d)

Fig. 6. Experiment 4 with perspective camera: left column when using closest pairing and right column when using farthest paring. (a) and (b)) translational velocities given in m/s, (c) and (d) rotational velocities given in rad/s

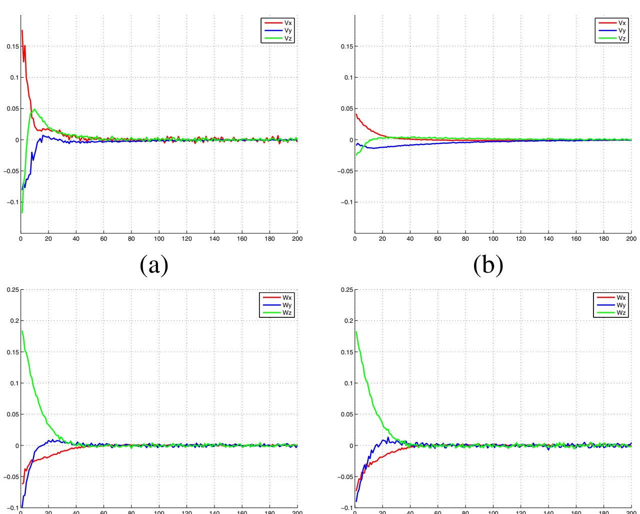

(a) (b) (c) (d)

Fig. 7. Experiment 4 with catadioptric camera: left column when using closest pairing and right column when using farthest paring. (a) and (b)) translational velocities given in m/s, (c) and (d) rotational velocities given in rad/s

REFERENCES

[1] L. Cordesses B. Thuilot, P. Martinet and J. Gallice. Position based visual servoing : keeping the object in the field of vision. In *IEEE Int. Conf. on Robotics and Automation, ICRA'02*, pages 1624–1629, Washington DC, USA,, May 2002.

[2] J. Barreto and H. Araujo. Geometric properties of central catadioptric line images. In *7th European Conference on Computer Vision, ECCV'02*, pages 237–251, Copenhagen, Denmark, May 2002.

[3] F. Chaumette. Potential problems of stability and convergence in image-based and position-based visual servoing. *The Confluence of Vision and Control, D. Kriegman, G. Hager, A. Morse (eds), LNCIS Series, Springer Verlag*, 237:66–78, 1998.

[4] F. Chaumette. Image moments: A general and useful set of features for visual servoing. *IEEE Transaction on Robotics and Automation*, 20(4):713–723, August 2004.

[5] P. I. Corke and S. A. Hutchinson. A new partitioned approach to image-based visual servo control. *IEEE Transaction on Robotics and Automation*, 17(4):507–515, August 2001.

[6] J. Courbon, Y. Mezouar, L. Eck, and P. Martinet. A generic fisheye camera model for robotic applications. In *IEEE/RSJ International Conference on Intelligent Robots and Systems*, San Diego, California, USA, 29 October 2 November 2007.

[7] B. Espiau, F. Chaumette, and P. Rives. A new approach to visual servoing in robotics. *IEEE Trans. on Robotics and Automation*, 8(3):313–326, June 1992.

[8] C. Geyer and K. Daniilidis. A unifying theory for central panoramic systems and practical implications. In *European Conference on Computer Vision*, volume 29, pages 159–179, Dublin, Ireland, May 2000.

[9] C. Geyer and K. Daniilidis. Mirrors in motion: Epipolar geometry and motion estimation. In *International Conference on Computer Vision, ICCV03*, pages 766–773, Nice, France, 2003.

[10] H. Hadj-Abdelkader, Y. Mezouar, N. Andreff, and P. Martinet. 2 1/2 d visual servoing with central catadioptric cameras. In *IEEE/RSJ Int. Conf. on Intelligent Robots and Systems, IROS'05*, pages 2342–2347, Edmonton, Canada, August 2005.

[11] T. Hamel and R. Mahony. Visual servoing of an under-actuated dynamic rigid body system: an image-based approach. *IEEE Transaction on Robotics and Automation*, 18(2):187–198, April 2002.

[12] M. Iwatsuki and N. Okiyama. A new formulation of visual servoing based on cylindrical coordinates system with shiftable origin. In *IEEE/RSJ International Conference on Intelligent Robots and Systems*, Lausanne, Switzerland, October 2002.

[13] J.-S. Lee, I.H. Suh, B.-J. You, and S.-R. Oh. A novel visual servoing approach involving disturbance observer. In *IEEE International Conference on Robotics and Automation, ICRA99*, pages 269–274, Detroit, Michigan, May 1999.

[14] E. Malis and F. Chaumette. 2 1/2 d visual servoing with respect to unknown objects through a new estimation scheme of camera displacement. *International Journal of Computer Vision*, 37(1):79–97, June 2000.

[15] E. Malis, F. Chaumette, and S. Boudet. 2 1/2 d visual servoing. *IEEE Transactions on Robotics and Automation*, 15(2):238–250, April 1999.

[16] P. Martinet, N. Daucher, J. Gallice, and M. Dhome. *Robot control using monocular pose estimation*. Worshop on New Trends in Image-based Robot Servoing, IROS'97, Grenoble, 1997.

[17] Y. Mezouar and F. Chaumette. Path planning for robust image-based control. *IEEE Transaction on Robotics and Automation*, 18(4):534–549, August 2002.

[18] P. Rives and J. Azinheira. Linear structures following by an airship using vanishing points and horizon line in a visual servoing scheme. In *IEEE International Conference on Robotics and Automation, ICRA04*, pages 255–260, New Orleans, Louisiana, April 2004.

[19] C. Samson, B. Espiau, and M. Le Borgne. *Robot Control : The Task Function Approach*. Oxford University Press, 1991.

[20] O. Tahri, F. Chaumette, and Y. Mezouar. New decoupled visual servoing scheme based on invariants projection onto a sphere. In *IEEE Int. Conf. on Robotics and Automation, ICRA'08*, Pasadena, CA, May 2008.

[21] R. Tatsambon Fomena and F. Chaumette. Visual servoing from spheres using a spherical projection model. In *IEEE International Conference on Robotics and Automation, ICRA'07*, Roma, Italia, April 2007.

[22] W.J Wilson, C.C Williams Hulls, and G.S Bell. Relative end-effector control using cartesian position-based visual servoing. *IEEE Trans. on Robotics and Automation*, 12(5):684–696, 1996.